

**Static, stationary, and inertial Unruh-DeWitt detectors on the BTZ black hole**Lee Hodgkinson<sup>1,\*</sup> and Jorma Louko<sup>1,2,†</sup><sup>1</sup>*School of Mathematical Sciences, University of Nottingham, Nottingham NG7 2RD, United Kingdom*<sup>2</sup>*Kavli Institute for Theoretical Physics, University of California, Santa Barbara, California 93106-4030, USA*

(Received 20 June 2012; published 18 September 2012)

We examine an Unruh-DeWitt particle detector coupled to a scalar field in three-dimensional curved spacetime. We first obtain a regulator-free expression for the transition probability in an arbitrary Hadamard state, working within first-order perturbation theory and assuming smooth switching, and we show that both the transition probability and the instantaneous transition rate remain well defined in the sharp switching limit. We then analyze a detector coupled to a massless conformally coupled field in the Hartle-Hawking vacua on the Bañados-Teitelboim-Zanelli black hole, under both transparent and reflective boundary conditions at the infinity. A selection of stationary and freely falling detector trajectories are examined, including the corotating trajectories, for which the response is shown to be thermal. Analytic results in a number of asymptotic regimes, including those of large and small mass, are complemented by numerical results in the interpolating regimes. The boundary condition at infinity is seen to have a significant effect on the transition rate.

DOI: [10.1103/PhysRevD.86.064031](https://doi.org/10.1103/PhysRevD.86.064031)

PACS numbers: 04.62.+v, 04.70.Dy

**I. INTRODUCTION**

The Unruh-DeWitt model for a particle detector [1,2] is an important tool for probing the physics of quantum fields wherever noninertial observers or curved backgrounds are present. In such cases there is often no distinguished notion of a “particle,” analogous to the plane-wave modes in Minkowski space, but an operational meaning can be attached to the particle concept by analyzing the transitions between the energy levels of a detector coupled to the field: upwards (respectively downwards) transitions can be interpreted as due to absorption (emission) of field quanta, or particles. The best-known applications of this procedure are those for which the spectrum of transitions is thermal, which is the case for uniformly linearly accelerated detectors in Minkowski space [1–4], detectors at rest in the exterior Schwarzschild black hole spacetime [5–7], and inertial detectors in de Sitter space [8].

With the Unruh-DeWitt detector, the fundamental quantity of interest is the probability of a transition between the energy eigenstates. In the framework of first-order perturbation theory this probability is proportional to the response function, given by a Fourier transform of the Wightman distribution of the quantum field over the detector’s worldline, weighted by a switching function that specifies how the interaction is turned on and off [9,10]. The response function is mathematically well defined provided the state of the quantum field is regular in the Hadamard sense [11,12] and the detector is switched on and off smoothly [13–16]. Physically, the response function then gives the probability for the detector to have

completed a quantum jump by the time the interaction with the field has ceased.

A related quantity of interest is the transition rate, which can be defined as the derivative of the transition probability with respect to the total detection time, and is observationally meaningful in terms of consequent measurements in identical ensembles of detectors [17]. There are technical subtleties in isolating in the transition rate the effects that are merely due to the switch-on and switch-off and the effects that are genuinely due to the acceleration and to the quantum state of the field [18–23]; however, a satisfactory treatment within first-order perturbation theory is to start with a smoothly switched detector and take a controlled sharp switching limit [17,24,25]. In particular, in three-dimensional Minkowski space, with a massless scalar field in the Minkowski vacuum, this procedure yields a finite result both for the transition probability and the transition rate even in the sharp switching limit [25].

In this paper we consider a detector in three-dimensional curved spacetime. In the first part of the paper we investigate a detector that is coupled to a scalar field in an arbitrary Hadamard state in an arbitrary spacetime. We give for the transition probability an expression that involves no distributional integrals, and we show that both the transition probability and the transition rate remain finite in the sharp switching limit. In the special case of a massless scalar field in the Minkowski vacuum of Minkowski spacetime, we recover the results of Ref. [25].

In the second part of the paper we apply the transition rate formula to a detector in the  $(2+1)$ -dimensional Bañados-Teitelboim-Zanelli (BTZ) black hole spacetime [26,27], for a massless conformally coupled scalar field in a Hartle-Hawking vacuum state [6,7,28,29] with transparent, Dirichlet or Neumann boundary conditions at the asymptotically anti-de Sitter infinity. We first consider a

\*[pmxhl1@nottingham.ac.uk](mailto:pmxhl1@nottingham.ac.uk)†[jorma.louko@nottingham.ac.uk](mailto:jorma.louko@nottingham.ac.uk)

stationary detector outside the hole, switched on in the asymptotic past. When the detector is corotating with the black hole horizon, we verify that the transition rate is thermal in the corotating local Hawking temperature, in the sense of the Kubo-Martin-Schwinger (KMS) property [30,31], as is to be expected from general properties of the Hartle-Hawking state [6,7,28,32] and also from global embedding space (GEMS) considerations [33–36]. We obtain analytic results in a number of asymptotic regimes, including those of large and small mass, and we provide numerical results in the interpolating regimes. A static detector outside a nonrotating black hole is included as a special case. When the detector is stationary but its angular velocity differs from that of the horizon, we find that the transition rate breaks the KMS property already to quadratic order in the difference of the angular velocities of the horizon and the detector.

We also consider a detector that falls into a nonrotating BTZ hole along a radial geodesic. We analyze the time evolution of the transition rate, obtaining analytic results for large black hole mass and large detector energy gap and numerical results in other regimes. We find no evidence of thermality in the transition rate, not even near the moment of maximum distance from the black hole, and we trace this phenomenon to the nonthermal response of an inertial detector in the corresponding vacuum state in pure anti-de Sitter space, as predicted from GEMS considerations [33–36].

We find that the boundary condition at the infinity has a significant effect on the transition rate for all of our detector trajectories. Typically, the Dirichlet condition gives a transition rate that varies least rapidly as a function of the detector’s energy gap and the total detection time, owing to partial cancellations between terms in the Dirichlet Wightman function. Similar cancellations do not occur for the Neumann or transparent boundary condition.

We begin in Sec. II with a brief review of the Unruh-DeWitt detector model, recalling, in particular, how the distributional character of the Wightman function needs to be addressed prior to taking a sharp switching limit. In Sec. III we consider an arbitrary Hadamard state in an arbitrary three-dimensional spacetime, writing the transition probability without distributional integrals and obtaining the formulas for the transition probability and the transition rate in the sharp switching limit. Section IV briefly reviews relevant properties of the BTZ black hole and the Hartle-Hawking vacua for a massless conformally coupled scalar field. A stationary detector is considered in Sec. V and a freely falling detector in Sec. VI. Section VII presents concluding remarks. Technical steps in contour integral analyses and asymptotic expansions are delegated to six appendices.

Our metric signature is  $(- + +)$ , and we use units in which  $c = \hbar = 1$ . Spacetime points are denoted by sans serif letters.  $O(x)$  denotes a quantity for which  $O(x)/x$  is

bounded as  $x \rightarrow 0$ ,  $o(x)$  denotes a quantity for which  $o(x)/x \rightarrow 0$  as  $x \rightarrow 0$ ,  $O(1)$  denotes a quantity that is bounded in the limit under consideration, and  $o(1)$  denotes a quantity that vanishes in the limit under consideration.

## II. UNRUH-DEWITT DETECTOR

In this section we briefly review the Unruh-DeWitt detector coupled to a scalar field, treated in first-order perturbation theory in the coupling [1,2].

The detector is an idealized atom with two energy levels, denoted by  $|0\rangle_d$  and  $|E\rangle_d$ , with the respective energy eigenvalues 0 and  $E$ , where  $E$  may be positive or negative. The detector is spatially pointlike and moves on a timelike worldline  $\mathbf{x}(\tau)$ , parametrized by the detector’s proper time  $\tau$ , in a spacetime of dimension two or higher. The detector interacts with a free real scalar field  $\phi$ , of arbitrary mass and curvature coupling, by the interaction Hamiltonian

$$H_{\text{int}} = c\chi(\tau)\mu(\tau)\phi(\mathbf{x}(\tau)), \quad (2.1)$$

where  $c$  is a small coupling constant and  $\mu(\tau)$  is the atom’s monopole moment operator.  $\chi$  is the switching function, positive during the interaction and vanishing elsewhere; this function specifies how the detector is switched on and off. We assume  $\chi$  to be smooth and of compact support, and we assume the trajectory to be smooth on the support of  $\chi$ .

Before the interaction begins, we assume the detector to be in the state  $|0\rangle_d$  and the field to be in a state  $|\Psi\rangle$ , and we assume  $|\Psi\rangle$  to be regular in the sense that it satisfies the Hadamard property [12]. The detector-field system is hence initially in the composite state  $|0\rangle_d \otimes |\Psi\rangle$ . We are interested in the probability for the detector to be found in the state  $|E\rangle_d$  after the interaction has ceased, regardless of the final state of the field. Working in first-order perturbation theory, this probability factorizes as [9,10]

$$P(E) = c^2 |{}_d\langle 0|\mu(0)|E\rangle_d|^2 \mathcal{F}(E), \quad (2.2)$$

where the response function  $\mathcal{F}(E)$  encodes the information about the detector’s trajectory, the initial state of the field, and the way the detector has been switched on and off.  $\mathcal{F}(E)$  can be expressed as [19]

$$\begin{aligned} \mathcal{F}(E) &= 2 \lim_{\epsilon \rightarrow 0_+} \text{Re} \int_{-\infty}^{\infty} du \chi(u) \\ &\times \int_0^{\infty} ds \chi(u-s) e^{-iEs} W_{\epsilon}(u, u-s), \end{aligned} \quad (2.3)$$

where  $W_{\epsilon}(u, u-s)$  is a one-parameter family of functions that converge to the pullback of the Wightman distribution to the detector’s worldline [11,13,14,17]. The factors in front of  $\mathcal{F}(E)$  in (2.2) depend only on the internal structure of the detector and we shall from now on drop them, referring to  $\mathcal{F}(E)$  as the transition probability.

In summary, the response function  $\mathcal{F}(E)$  answers the question, “What is the probability of the detector to be observed in the state  $|E\rangle_d$  after the interaction has ceased?”

Given  $\mathcal{F}(E)$ , we may define the detector's "transition rate" as the derivative of  $\mathcal{F}(E)$  with respect to the total detection time [19,23]. Both  $\mathcal{F}(E)$  and the transition rate depend not only on the initial state of the field and the detector's trajectory but also on the switching, and their behavior in the sharp switching limit depends sensitively on the space-time dimension [25].

Working directly with the expression (2.3) for  $\mathcal{F}(E)$  is cumbersome because the limit  $\epsilon \rightarrow 0_+$  may not necessarily be taken pointwise under the integral [17,19–25]. In Sec. III we shall address this issue in three spacetime dimensions.

### III. TRANSITION PROBABILITY AND TRANSITION RATE IN THREE SPACETIME DIMENSIONS

In this section we specialize to three spacetime dimensions. We first rewrite the response function (2.3) in a form in which the regulator  $\epsilon$  does not appear. We then take the sharp switching limit and show that both the transition probability and the transition rate remain well defined in this limit. We follow closely the procedure developed in Refs. [17,23–25].

#### A. Hadamard form of $W_\epsilon$

In a three-dimensional spacetime, the Wightman distribution  $W(\mathbf{x}, \mathbf{x}')$  of a real scalar field in a Hadamard state can be represented by a family of functions with the short distance form [12]

$$W_\epsilon(\mathbf{x}, \mathbf{x}') = \frac{1}{4\pi} \left[ \frac{U(\mathbf{x}, \mathbf{x}')}{\sqrt{\tilde{\sigma}_\epsilon(\mathbf{x}, \mathbf{x}')}} + \frac{H(\mathbf{x}, \mathbf{x}')}{\sqrt{2}} \right], \quad (3.1)$$

where  $\epsilon$  is a positive parameter,  $\tilde{\sigma}(\mathbf{x}, \mathbf{x}')$  is the squared geodesic distance between  $\mathbf{x}$  and  $\mathbf{x}'$ ,  $\tilde{\sigma}_\epsilon(\mathbf{x}, \mathbf{x}') := \tilde{\sigma}(\mathbf{x}, \mathbf{x}') + 2i\epsilon[T(\mathbf{x}) - T(\mathbf{x}')] + \epsilon^2$ , and  $T$  is any globally defined future-increasing  $C^\infty$  function. The branch of the square root is such that the  $\epsilon \rightarrow 0_+$  limit of the square root is positive when  $\tilde{\sigma}(\mathbf{x}, \mathbf{x}') > 0$  [11,12]. Here  $U(\mathbf{x}, \mathbf{x}')$  and  $H(\mathbf{x}, \mathbf{x}')$  are symmetric biscalars that possess expansions of the form

$$U(\mathbf{x}, \mathbf{x}') = \sum_{n=0}^{\infty} U_n(\mathbf{x}, \mathbf{x}') \sigma^n(\mathbf{x}, \mathbf{x}'), \quad (3.2a)$$

$$H(\mathbf{x}, \mathbf{x}') = \sum_{n=0}^{\infty} H_n(\mathbf{x}, \mathbf{x}') \sigma^n(\mathbf{x}, \mathbf{x}'), \quad (3.2b)$$

where the coefficients  $U_n(\mathbf{x}, \mathbf{x}')$  satisfy the recursion relations

$$\begin{aligned} (n+1)(2n+1)U_{n+1} + (2n+1)U_{n+1;\mu} \sigma^{;\mu} \\ - (2n+1)U_{n+1} \Delta^{-1/2} \Delta^{1/2}_{;\mu} \sigma^{;\mu} \\ + (\square_x - m^2 - \xi R)U_n = 0, \\ n = 0, 1, 2, \dots, \end{aligned} \quad (3.3)$$

with the boundary condition

$$U_0 = \Delta^{1/2}, \quad (3.4)$$

and the coefficients  $H_n(\mathbf{x}, \mathbf{x}')$  satisfy the recursion relations

$$\begin{aligned} (n+1)(2n+3)H_{n+1} + 2(n+1)H_{n+1;\mu} \sigma^{;\mu} \\ - 2(n+1)H_{n+1} \Delta^{-1/2} \Delta^{1/2}_{;\mu} \sigma^{;\mu} \\ + (\square_x - m^2 - \xi R)H_n = 0, \\ n = 0, 1, 2, \dots, \end{aligned} \quad (3.5)$$

where  $\sigma = \frac{1}{2}\tilde{\sigma}$ ,  $\Delta(\mathbf{x}, \mathbf{x}')$  is the Van Vleck determinant,  $m$  is the mass, and  $\xi$  is the curvature coupling parameter [12].

The  $i\epsilon$  prescription in (3.1) defines the singular part of  $W(\mathbf{x}, \mathbf{x}')$ : the action of the Wightman distribution is obtained by integrating  $W_\epsilon(\mathbf{x}, \mathbf{x}')$  against test functions and taking the limit  $\epsilon \rightarrow 0_+$  as in (2.3). This limit can be shown to be independent of the choice of global time function  $T$  [13–16].

#### B. Transition probability without $i\epsilon$ regulator

To evaluate the  $\epsilon \rightarrow 0_+$  limit in (2.3), the main issue is at  $s = 0$ , where the Hadamard expansion (3.1) shows that the integrand develops a nonintegrable singularity as  $\epsilon \rightarrow 0_+$ . We shall work under the assumption that any other singularities that the integrand develops as  $\epsilon \rightarrow 0_+$  are integrable. This will be the case in our applications in Secs. V and VI. We note in passing that similar integrable singularities can occur in any space-time dimension, and the four-dimensional results in Ref. [17] should hence be understood to involve a similar assumption.

We first split the  $s$  integral in (2.3) into the subintervals  $(0, \eta)$  and  $(\eta, \infty)$  where  $\eta = \sqrt{\epsilon}$ . We then find the small  $\epsilon$  expansions of each integral and finally combine the results.

Let  $I_>$  denote the  $s \in (\eta, \infty)$  portion of the  $s$  integral in (2.3), including the taking of the real part. Let  $W_0$  denote the pointwise limit of  $W_\epsilon$  as  $\epsilon \rightarrow 0_+$ . Replacing  $W_\epsilon$  by  $W_0$  creates in  $I_>$  the error

$$\begin{aligned} 2 \operatorname{Re} \int_{\eta}^{\infty} ds \chi(u-s) e^{-iEs} [W_\epsilon(u, u-s) - W_0(u, u-s)] \\ = \frac{1}{2\pi} \operatorname{Re} \int_{\eta}^{\infty} ds \chi(u-s) e^{-iEs} U(u, u-s) \\ \times \left[ \frac{1}{\sqrt{\tilde{\sigma} + 2i\epsilon\Delta T + \epsilon^2}} + \frac{i}{\sqrt{-\tilde{\sigma}}} \right], \end{aligned} \quad (3.6)$$

where  $\tilde{\sigma}$  is evaluated at the pair  $(\mathbf{x}, \mathbf{x}') = (\mathbf{x}(u), \mathbf{x}(u-s))$ ,  $\Delta T := T(\mathbf{x}(u)) - T(\mathbf{x}(u-s))$ , and we recall that  $\tilde{\sigma} < 0$  as the trajectory is timelike. The square brackets in (3.6) have the same form as in the Minkowski analysis in Ref. [25] and obey similar estimates. The function  $U$  has the small  $s$  expansion

$$U(u, u-s) = 1 + O(s^2), \quad (3.7)$$

by virtue of (3.2a), (3.4), and the expansions  $\tilde{\sigma} = -s^2 + O(s^4)$  and  $\Delta = 1 + O(s^2)$ . These observations show that the contribution from (3.6) to  $I_>$  is  $O(\eta)$ . We hence have

$$I_> = 2 \int_0^\infty ds \chi(u-s) \text{Re}[e^{-iEs} W_0(u, u-s)] + O(\eta), \quad (3.8)$$

where we have extended the lower limit to 0 at the expense of an error that is contained in the  $O(\eta)$  term since (3.1) shows that taking the real part under the integral makes the integrand regular at  $s = 0$ .

Let then  $I_<$  denote the  $s \in (0, \eta)$  portion of the  $s$  integral in (2.3), including the taking of the real part. We have

$$\begin{aligned} I_< &= 2 \text{Re} \int_0^\eta ds \chi(u-s) e^{-iEs} W_\epsilon(u, u-s) \\ &= \frac{1}{2\pi} \text{Re} \int_0^\eta ds \chi(u-s) e^{-iEs} \\ &\quad \times \left[ \frac{U(u, u-s)}{\sqrt{\tilde{\sigma} + 2i\epsilon\Delta T + \epsilon^2}} + \frac{H(u, u-s)}{\sqrt{2}} \right]. \end{aligned} \quad (3.9)$$

Since  $H(u, u-s)$  is a regular function, its contribution to  $I_<$  is  $O(\eta)$ . The contribution of the term involving  $U$  can be found using the estimates of [25] and the expansion (3.7). We find

$$I_< = \chi(u)/4 + O(\eta). \quad (3.10)$$

Combining (3.8) and (3.10), and noting that their error estimates hold uniformly in  $u$ , it is immediate to take the  $\epsilon \rightarrow 0_+$  limit in (2.3). We find

$$\begin{aligned} \mathcal{F}(E) &= \frac{1}{4} \int_{-\infty}^\infty du [\chi(u)]^2 + 2 \int_{-\infty}^\infty du \chi(u) \\ &\quad \times \int_0^\infty ds \chi(u-s) \text{Re}[e^{-iEs} W_0(u, u-s)]. \end{aligned} \quad (3.11)$$

Note that the integrals in (3.11) are regular, at  $s = 0$  by the Hadamard short-distance behavior of  $W_0$ , and at  $s > 0$  by our assumptions about the singularity structure of  $W_0$  at timelike-separated points.

### C. Sharp switching limit and the transition rate

Up to now we have assumed the switching function  $\chi$  to be smooth. When  $\chi$  approaches the characteristic function of the interval  $[\tau_0, \tau_0 + \tau]$  in a sufficiently controlled fashion [17, 24, 25], the integrands in (3.11) remain regular and taking the sharp switching limit under the integral can be justified by dominated convergence. The transition probability takes the form

$$\mathcal{F}_\tau(E) = \frac{\Delta\tau}{4} + 2 \int_{\tau_0}^\tau du \int_0^{u-\tau_0} ds \text{Re}[e^{-iEs} W_0(u, u-s)], \quad (3.12)$$

where  $\Delta\tau := \tau - \tau_0$  and the subscript  $\tau$  is included as a reminder of the dependence on the switch-off moment. Differentiation with respect to  $\tau$  shows that the transition rate is given by

$$\dot{\mathcal{F}}_\tau(E) = \frac{1}{4} + 2 \int_0^{\Delta\tau} ds \text{Re}[e^{-iEs} W_0(\tau, \tau-s)]. \quad (3.13)$$

Note that both (3.12) and (3.13) are well defined under our assumptions, and in the special case of a massless scalar field in the Minkowski vacuum they reduce to what was found in Ref. [25]. Spacetime curvature has hence not introduced new singularities in the sharp switching limit.

Note also that the preintegral term  $\frac{1}{4}$  in (3.13) would have been missed if the limit  $\epsilon \rightarrow 0_+$  had been taken naively under the integral in (2.3). Yet this term is essential: it was observed in Ref. [25] that without this term one would not recover the standard thermal response for a uniformly linearly accelerated detector in Minkowski vacuum [3, 37], and we shall see in Sec. V that without this term we would not recover thermality for a corotating detector in the BTZ spacetime.

## IV. DETECTOR IN THE BTZ SPACETIME

We now turn to a detector in the BTZ black hole spacetime [26, 27], specializing to a massless conformally coupled scalar field in the Hartle-Hawking vacuum with transparent or reflective boundary conditions. In this section we briefly recall relevant properties of the spacetime and the Wightman function. More detail can be found in the review in Ref. [29].

Recall first that three-dimensional anti-de Sitter spacetime  $\text{AdS}_3$  may be defined as the submanifold

$$-\ell^2 = -T_1^2 - T_2^2 + X_1^2 + X_2^2, \quad (4.1)$$

in  $\mathbb{R}^{2,2}$  with coordinates  $(T_1, T_2, X_1, X_2)$  and metric

$$dS^2 = -dT_1^2 - dT_2^2 + dX_1^2 + dX_2^2, \quad (4.2)$$

where  $\ell$  is a positive parameter of dimension length. The BTZ black hole is obtained as a quotient of an open region in  $\text{AdS}_3$  under a discrete isometry group  $\simeq \mathbb{Z}$ . Specializing to a nonextremal black hole, a set of coordinates that are adapted to the relevant isometries and cover the exterior region of the black hole are the BTZ coordinates  $(t, r, \phi)$ , defined in  $\text{AdS}_3$  by

$$\begin{aligned} X_1 &= \ell \sqrt{\alpha} \sinh\left(\frac{r_+}{\ell} \phi - \frac{r_-}{\ell^2} t\right), \\ X_2 &= \ell \sqrt{\alpha - 1} \cosh\left(\frac{r_+}{\ell^2} t - \frac{r_-}{\ell} \phi\right), \\ T_1 &= \ell \sqrt{\alpha} \cosh\left(\frac{r_+}{\ell} \phi - \frac{r_-}{\ell^2} t\right), \\ T_2 &= \ell \sqrt{\alpha - 1} \sinh\left(\frac{r_+}{\ell^2} t - \frac{r_-}{\ell} \phi\right), \end{aligned} \quad (4.3)$$



where

$$\alpha(r) = \left( \frac{r^2 - r_-^2}{r_+^2 - r_-^2} \right), \quad (4.4)$$

and the parameters  $r_{\pm}$  satisfy  $|r_-| < r_+$ . The coordinate ranges covering the black hole exterior are  $r_+ < r < \infty$ ,  $-\infty < t < \infty$ , and  $-\infty < \phi < \infty$ , and the  $\mathbb{Z}$  quotient is realized as the identification  $(t, r, \phi) \sim (t, r, \phi + 2\pi)$ . The outer horizon is at  $r \rightarrow r_+$ , and the asymptotically AdS<sub>3</sub> infinity is at  $r \rightarrow \infty$ . The metric takes the form

$$ds^2 = -(N^\perp)^2 dt^2 + f^{-2} dr^2 + r^2 (d\phi + N^\phi dt)^2, \quad (4.5)$$

with

$$N^\perp = f = \left( -M + \frac{r^2}{\ell^2} + \frac{J^2}{4r^2} \right)^{1/2}, \quad N^\phi = -\frac{J}{2r^2}, \quad (4.6)$$

where the mass  $M$  and the angular momentum  $J$  are given by

$$M = (r_+^2 + r_-^2)/\ell^2, \quad J = 2r_+ r_-/\ell, \quad (4.7)$$

and they satisfy  $|J| < M\ell$ .

In a quantum state invariant under  $\partial_\phi$ , the Wightman function on the black hole spacetime can be expressed as an image sum of the corresponding AdS<sub>3</sub> Wightman function. If  $G_A(\mathbf{x}, \mathbf{x}')$  denotes the AdS<sub>3</sub> Wightman function, the BTZ Wightman function reads [29]

$$G_{\text{BTZ}}(\mathbf{x}, \mathbf{x}') = \sum_n G_A(\mathbf{x}, \Lambda^n \mathbf{x}'), \quad (4.8)$$

where  $\Lambda \mathbf{x}'$  denotes the action on  $\mathbf{x}'$  of the group element  $(t, r, \phi) \mapsto (t, r, \phi + 2\pi)$ , and the notation suppresses the distinction between points on AdS<sub>3</sub> and points on the quotient spacetime. The scalar field is assumed untwisted so that no additional phase factors appear in (4.8).

We consider a massless, conformally coupled field, and the family of AdS<sub>3</sub> Wightman functions [29]

$$G_A^{(\zeta)}(\mathbf{x}, \mathbf{x}') = \frac{1}{4\pi} \left( \frac{1}{\sqrt{\Delta X^2(\mathbf{x}, \mathbf{x}')}} - \frac{\zeta}{\sqrt{\Delta X^2(\mathbf{x}, \mathbf{x}') + 4\ell^2}} \right), \quad (4.9)$$

where the parameter  $\zeta \in \{0, 1, -1\}$  specifies whether the boundary condition at infinity is respectively transparent, Dirichlet or Neumann. Here  $\Delta X^2(\mathbf{x}, \mathbf{x}')$  is the squared geodesic distance between  $\mathbf{x}$  and  $\mathbf{x}'$  in the flat embedding spacetime  $\mathbb{R}^{2,2}$ , given by

$$\begin{aligned} \Delta X^2(\mathbf{x}, \mathbf{x}') &:= -(T_1 - T'_1)^2 - (T_2 - T'_2)^2 \\ &\quad + (X_1 - X'_1)^2 + (X_2 - X'_2)^2, \end{aligned} \quad (4.10)$$

and we have momentarily suppressed the  $i\epsilon$  prescription in (4.9).

With (4.8) and (4.9), the transition rate (3.13) takes the form

$$\begin{aligned} \dot{\mathcal{F}}_\tau(E) &= \frac{1}{4} + \frac{1}{2\pi\sqrt{2}} \sum_{n=-\infty}^{\infty} \int_0^{\Delta\tau/\ell} d\tilde{s} \\ &\quad \times \text{Re} \left[ e^{-iE\ell\tilde{s}} \left( \frac{1}{\sqrt{\Delta\tilde{X}_n^2}} - \frac{\zeta}{\sqrt{\Delta\tilde{X}_n^2 + 2}} \right) \right], \end{aligned} \quad (4.11)$$

where we have introduced the dimensionless integration variable  $\tilde{s} := s/\ell$  and written

$$\begin{aligned} \Delta\tilde{X}_n^2 &:= \Delta X^2(\mathbf{x}(\tau), \Lambda^n \mathbf{x}(\tau - \ell\tilde{s})) / (2\ell^2) \\ &= -1 + \sqrt{\alpha(r)\alpha(r')} \cosh[(r_+/\ell)(\phi - \phi' - 2\pi n) \\ &\quad - (r_-/\ell^2)(t - t')] - \sqrt{(\alpha(r) - 1)(\alpha(r') - 1)} \\ &\quad \times \cosh[(r_+/\ell^2)(t - t') - (r_-/\ell)(\phi - \phi' - 2\pi n)], \end{aligned} \quad (4.12)$$

where the unprimed coordinates are evaluated at  $\mathbf{x}(\tau)$  and the primed coordinates at  $\mathbf{x}(\tau - \ell\tilde{s})$ .

What remains is to specify the branches of the square roots in (4.11). As  $s$  extends to a global time function in the relevant part of AdS<sub>3</sub>, the prescription (3.1) implies that the square roots in (4.11) are positive when the arguments are positive, and the square roots are analytically continued to negative values of the arguments by giving  $s$  a small negative imaginary part.

## V. COROTATING DETECTOR IN BTZ

In this section we investigate the transition rate of a detector that is in the exterior region of the BTZ black hole and corotating with the horizon. As the detector is stationary, we take the switch-on to be in the asymptotic past. When the black hole is spinless, the detector is static.

### A. Transition rate and the KMS property

The angular velocity of the horizon is given by [26,27,29]

$$\Omega_H = r_-/(r_+\ell), \quad (5.1)$$

and it has an operational meaning as the value that  $d\phi/dt$  takes on any timelike worldline that crosses the horizon. The worldline of a detector that is in the exterior region and rigidly corotating with the horizon reads

$$\begin{aligned} r &= \text{constant}, \quad t = \frac{\ell r_+ \tau}{\sqrt{r^2 - r_+^2} \sqrt{r_+^2 - r_-^2}}, \\ \phi &= \frac{r_- \tau}{\sqrt{r^2 - r_+^2} \sqrt{r_+^2 - r_-^2}}, \end{aligned} \quad (5.2)$$

where the value of  $r$  specifies the radial location and  $\tau$  is the proper time. We have set the additive constants in  $t$  and  $\phi$  to zero without loss of generality.

Substituting (5.2) into (4.12) and taking the switch-on to be in the asymptotic past, the transition rate (4.11) takes the form

$$\dot{\mathcal{F}}(E) = \frac{1}{4} + \frac{1}{4\pi\sqrt{\alpha(r)-1}} \sum_{n=-\infty}^{\infty} \int_0^{\infty} d\tilde{s} \operatorname{Re} \left[ e^{-iE\tilde{s}} \left( \frac{1}{\sqrt{K_n - \sinh^2(\Xi\tilde{s} + n\pi r_-/\ell)}} - \frac{\zeta}{\sqrt{Q_n - \sinh^2(\Xi\tilde{s} + n\pi r_-/\ell)}} \right) \right], \quad (5.3)$$

where

$$K_n := (1 - \alpha^{-1})^{-1} \sinh^2(n\pi r_+/\ell), \quad (5.4a)$$

$$Q_n := K_n + (\alpha - 1)^{-1}, \quad (5.4b)$$

$$\Xi := (2\sqrt{\alpha - 1})^{-1}, \quad (5.4c)$$

$\alpha$  is given by (4.4), and we have dropped the subscript  $\tau$  from  $\dot{\mathcal{F}}$  as the situation is stationary and the transition rate is independent of  $\tau$ . The square roots in (5.3) are positive for positive values of the argument, and they are analytically continued to negative values of the argument by giving  $\tilde{s}$  a small negative imaginary part. Note that the integrand in (5.3) has singularities at  $\tilde{s} > 0$ , at places where the quantity under a square root changes sign, but all of these singularities are integrable.

We show in Appendix A that (5.3) can be written as

$$\dot{\mathcal{F}}(E) = \frac{e^{-\beta E\ell/2}}{2\pi} \sum_{n=-\infty}^{\infty} \cos(n\beta E r_-) \int_0^{\infty} dy \cos(y\beta E\ell/\pi) \times \left( \frac{1}{\sqrt{K_n + \cosh^2 y}} - \frac{\zeta}{\sqrt{Q_n + \cosh^2 y}} \right), \quad (5.5)$$

or alternatively as

$$\dot{\mathcal{F}}(E) = \frac{1}{2(e^{\beta E\ell} + 1)} - \frac{\zeta e^{-\beta E\ell/2}}{2\pi} \int_0^{\infty} dy \frac{\cos(y\beta E\ell/\pi)}{\sqrt{Q_0 + \cosh^2 y}} + \frac{e^{-\beta E\ell/2}}{\pi} \sum_{n=1}^{\infty} \cos(n\beta E r_-) \int_0^{\infty} dy \cos(y\beta E\ell/\pi) \times \left( \frac{1}{\sqrt{K_n + \cosh^2 y}} - \frac{\zeta}{\sqrt{Q_n + \cosh^2 y}} \right), \quad (5.6)$$

where

$$\beta := 2\pi\sqrt{\alpha - 1}. \quad (5.7)$$

It is evident from (5.5) or (5.6) that  $\dot{\mathcal{F}}$  depends on  $E$  only via the dimensionless combination  $\ell\beta E$ . It is further evident that  $\dot{\mathcal{F}}$  has the KMS property [30,31]

$$\dot{\mathcal{F}}(E) = e^{-\ell\beta E} \dot{\mathcal{F}}(-E). \quad (5.8)$$

The transition rate is hence thermal in the temperature  $(\ell\beta)^{-1}$ .

It can be verified that  $(\ell\beta)^{-1} = (-g_{00})^{-1/2} T_0$ , where  $T_0 = \kappa_0/(2\pi)$ ,  $\kappa_0$  is the surface gravity of the black hole with respect to the horizon-generating Killing vector  $\partial_t + \Omega_H \partial_\phi$ , and  $g_{00}$  is the time-time component of the metric in coordinates adapted to the corotating observers. This means that the temperature  $(\ell\beta)^{-1}$  of the detector response is the local Hawking temperature, obtained by renormalizing the conventional Hawking temperature  $T_0$  by the

Tolman redshift factor at the detector's location. This is the temperature one would have expected by general properties of the Hartle-Hawking state [6,7,28], including the periodicity of an appropriately defined imaginary time coordinate [32], and also by GEMS considerations [33–36].

Note that the expressions (5.5) and (5.6) contain both terms of (3.13), as shown in Appendix A. The preintegral term  $\frac{1}{4}$  in (3.13) is hence essential for recovering thermality: in (5.6) it can be regarded as having been grouped in the term  $\frac{1}{2}(e^{\beta E\ell} + 1)^{-1}$ , which gives the transition rate in pure AdS<sub>3</sub> with the transparent boundary condition. The superficial Fermi-Dirac appearance of this pure AdS<sub>3</sub> term is a general feature of linearly coupled scalar fields in odd spacetime dimensions [3,28,37,38].

## B. Asymptotic regimes

We consider the behavior of the transition rate (5.6) in three asymptotic regimes.

First, suppose  $r_+ \rightarrow \infty$  so that  $r_-/r_+$  and  $r/r_+$  are fixed. Physically, this is the limit of a large black hole with fixed  $J/M$ , and the detector is assumed not to be close to the black hole horizon. Note that  $\alpha$  and  $\beta$  remain fixed in this limit. It follows from (4.4) and (5.4) that in (5.6) this is the limit in which  $K_n$  and  $Q_n$  with  $n \geq 1$  are large. Assuming that  $E$  is fixed and nonzero, and using formula (B2a) in Appendix B, we find

$$\dot{\mathcal{F}}(E) = \frac{1}{2(e^{\beta E\ell} + 1)} - \frac{\zeta e^{-\beta E\ell/2}}{2\pi} \times \int_0^{\infty} dy \frac{\cos(y\beta E\ell/\pi)}{\sqrt{Q_0 + \cosh^2 y}} + \frac{e^{-\beta E\ell/2} \cos(\beta E r_-)}{\sqrt{\pi}\beta E\ell} \times \left\{ \operatorname{Im} \left[ \left( \frac{(4K_1)^{i\beta E\ell/(2\pi)}}{\sqrt{K_1}} - \frac{\zeta(4Q_1)^{i\beta E\ell/(2\pi)}}{\sqrt{Q_1}} \right) \right] \times \Gamma\left(1 + \frac{i\beta E\ell}{2\pi}\right) \Gamma\left(\frac{1}{2} - \frac{i\beta E\ell}{2\pi}\right) \right\} + O(e^{-2\pi r_+/\ell}), \quad (5.9)$$

where the displayed next-to-leading term comes from the  $n = 1$  term in (5.6) and is of order  $e^{-\pi r_+/\ell}$ . The corresponding formula for  $E = 0$  can be obtained from formula (B2b) in Appendix B and has a next-to-leading term of order  $r_+ e^{-\pi r_+/\ell}$ .

Next, suppose that  $r_+ \rightarrow 0$  so that  $r_-/r_+$  and  $r/r_+$  are again fixed. This is the limit of a small black hole. Note that  $\alpha$  and  $\beta$  are again fixed. The dominant behavior comes now from the sum over  $n$  and can be estimated by the Riemann sum technique of Appendix C. We find

$$\begin{aligned} \mathcal{F}(E) = & \frac{\ell e^{-\beta E \ell/2}}{\pi^2 r_+} \int_0^\infty dv \int_0^\infty dy \cos\left(\frac{v \beta E \ell r_-}{\pi r_+}\right) \\ & \times \cos\left(\frac{y \beta E \ell}{\pi}\right) \times \left[ \left( \frac{\alpha \sinh^2 v}{(\alpha-1)} + \cosh^2 y \right)^{-1/2} \right. \\ & \left. - \zeta \left( \frac{1 + \alpha \sinh^2 v}{(\alpha-1)} + \cosh^2 y \right)^{-1/2} \right] + \frac{o(1)}{r_+}. \end{aligned} \quad (5.10)$$

The leading term is proportional to  $1/r_+$  and it hence diverges in the limit of a small black hole.

Finally, suppose that  $E \rightarrow \pm\infty$  with the other quantities fixed. The analysis of Appendix D shows that each integral term in (5.6) is oscillatory in  $E$ , with an envelope that falls off as  $1/\sqrt{-E}$  at  $E \rightarrow -\infty$  but exponentially at  $E \rightarrow +\infty$ . Applying this estimate to the lowest few values of  $n$  in (5.6) should be a good estimate to the whole sum when  $r_+/\ell$  is large. We have not attempted to estimate the whole sum at  $E \rightarrow \pm\infty$  when  $r_+/\ell$  is small.

### C. Numerical results

We now turn to a numerical evaluation of the transition rate (5.6). We are particularly interested in the interpolation between the asymptotic regimes identified in Sec. VB.

$\mathcal{F}$  (5.6) depends on five independent variables. Two of these are the mass and the angular momentum of the black hole, encoded in the dimensionless parameters  $r_+/\ell$  and  $r_-/\ell$ . The third is the location of the detector, entering  $\mathcal{F}$  only in the dimensionless combination  $\alpha$  (4.4). The fourth is the detector's energy gap  $E$ , entering  $\mathcal{F}$  only in the dimensionless combination  $\beta E \ell$  where  $\beta$  was given in (5.7). The last one is the discrete parameter  $\zeta \in \{0, 1, -1\}$ , which specifies the boundary condition at infinity.

We plot  $\mathcal{F}$  as a function of  $\ell \beta E$ , grouping the plots in triplets where  $\zeta$  runs over its three values and the other three parameters are fixed. We proceed from large  $r_+/\ell$  towards small  $r_+/\ell$ .

In the regime  $r_+/\ell \gtrsim 3$ , numerics confirms that the  $n \geq 1$  terms in (5.6) are small.  $\mathcal{F}$  therefore depends on  $r_+/\ell$  and  $r_-/\ell$  significantly only through  $\beta$ , that is, through the local temperature. The detector's location enters  $\mathcal{F}$  in part via  $\beta$  (5.7), but also via  $Q_0$  in (5.6), and the latter affects only the boundary conditions  $\zeta = 1$  and  $\zeta = -1$ , in opposite directions. Plots for  $r_+/\ell = 10$  are shown in Fig. 1.

As  $r_+/\ell$  decreases, the  $n = 1$  term in (5.6) starts to become appreciable near  $r_+/\ell \approx 1$ . The dependence on  $r_-/\ell$  is then no longer exclusively through  $\beta$ , and the effect is largest for  $\zeta = 0$  and  $\zeta = -1$  but smaller for  $\zeta = 1$ , owing to a partial cancellation between the two terms under the integral in (5.6) for  $\zeta = 1$ . Plots for  $r_+/\ell = 1$  are shown in Figs. 2 and 3.

As  $r_+/\ell$  decreases below 1, the next-to-leading asymptotic formula (5.9) starts to become inaccurate near  $r_+/\ell = 0.3$ , as shown in Fig. 4, although the partial cancellation between the two terms under the integral in (5.6) and the similar partial cancellation in (5.9) moderates the effect for  $\zeta = 1$ . At  $r_+/\ell = 0.1$ , shown in Fig. 5,  $\mathcal{F}$  is sensitive to changes in both  $r_-/\ell$  and  $\alpha$ . When  $\alpha \gg 1$ , the  $\zeta = -1$  curves in Fig. 5 have approximately the same profile as the  $\zeta = 0$  curves but at twice the magnitude: from (5.4a) and (5.4b) we see that this indicates the regime where the  $n \geq 1$  terms in (5.6) give the dominant contribution to  $\mathcal{F}$ .

As  $r_+/\ell$  decreases further, we enter the validity regime of the asymptotic formula (5.10), as shown in Fig. 6 for  $r_+/\ell = 0.01$ . Note that again the  $\zeta = -1$  curve has approximately the same profile as the  $\zeta = 0$  curve but at twice the magnitude, indicating that the dominant contribution comes from the  $n \geq 1$  terms in (5.6).

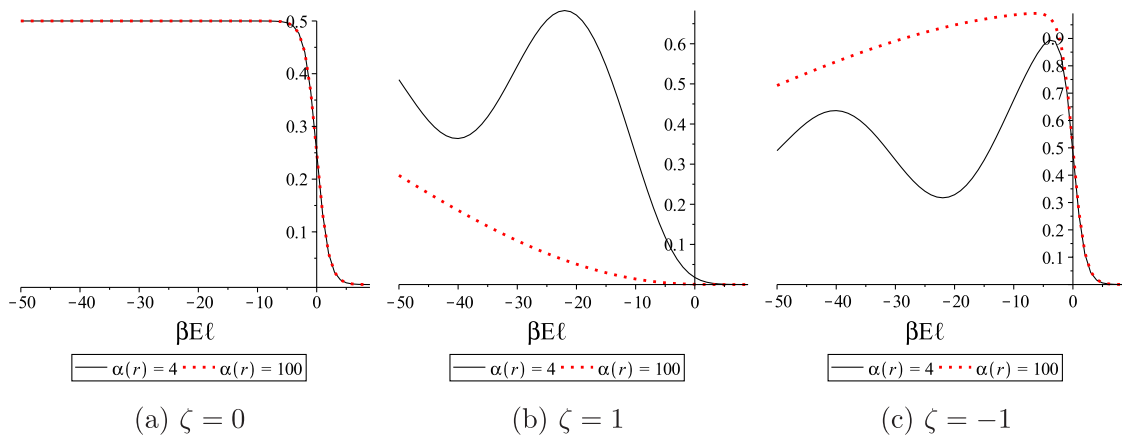


FIG. 1 (color online).  $\mathcal{F}$  as a function of  $\beta E \ell$  for  $r_+/\ell = 10$  and  $r_-/\ell = 0$ , with  $\alpha = 4$  (solid line) and  $\alpha = 100$  (dotted line). Numerical evaluation from (5.6) with  $n \leq 3$ .

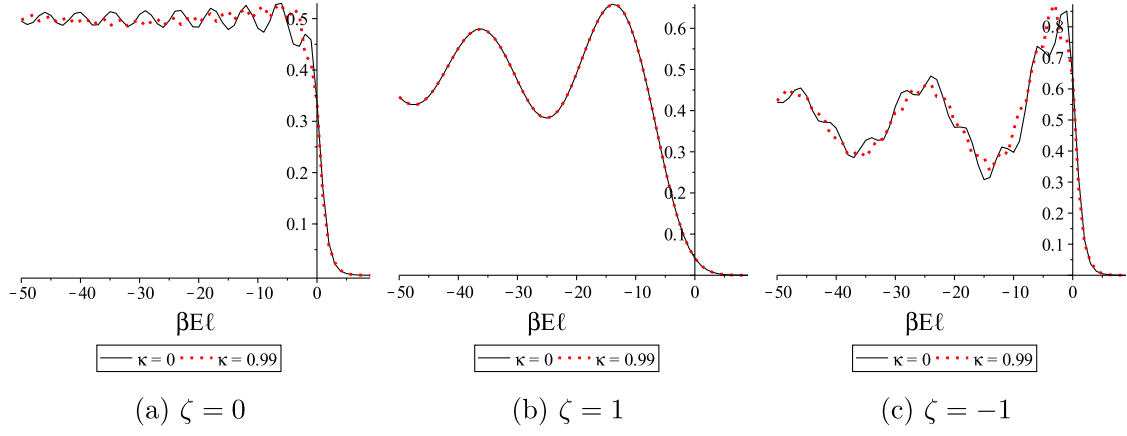


FIG. 2 (color online).  $\mathcal{F}$  as a function of  $\beta\ell$  for  $r_+/\ell = 1$  and  $\alpha = 2$ , with  $\kappa = 0$  (solid line) and  $\kappa = 0.99$  (dotted line) where  $\kappa := r_-/r_+$ . Numerical evaluation from (5.6) with  $n \leq 3$ .

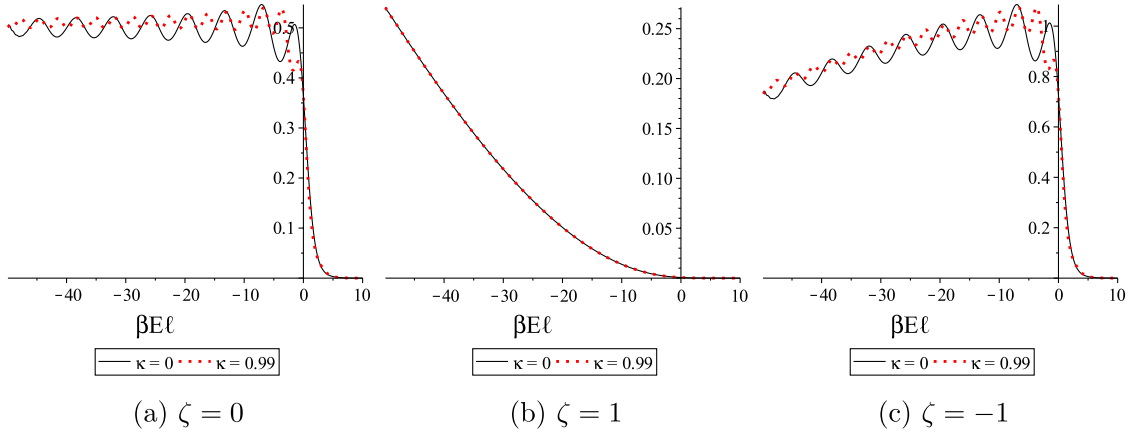


FIG. 3 (color online). As in Fig. 2 but for  $\alpha = 100$ .

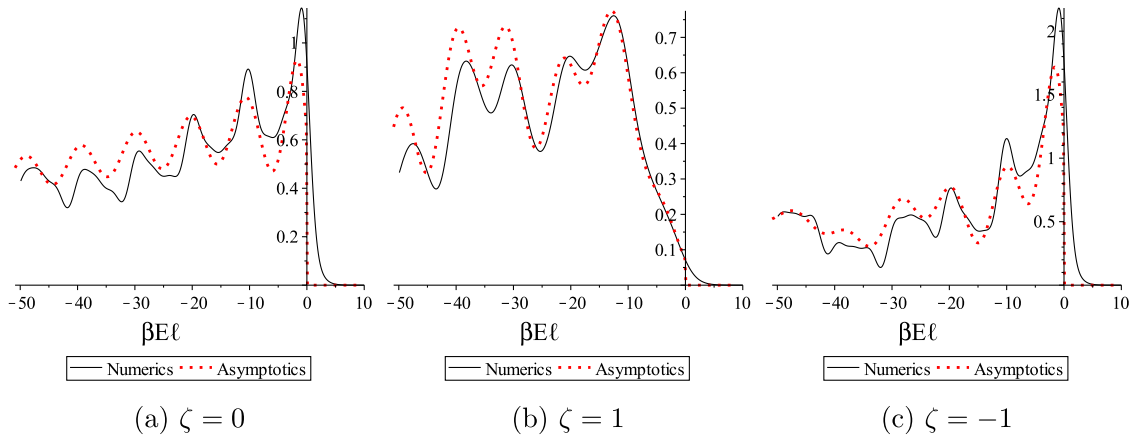


FIG. 4 (color online).  $\mathcal{F}$  as a function of  $\beta\ell$  for  $r_+/\ell = 0.3$  and  $r_-/\ell = 0.299$ , with  $\alpha = 2$ . Solid curve shows numerical evaluation from (5.6) with  $n \leq 3$ . Dotted curve shows the asymptotic large  $r_+/\ell$  approximation (5.9).



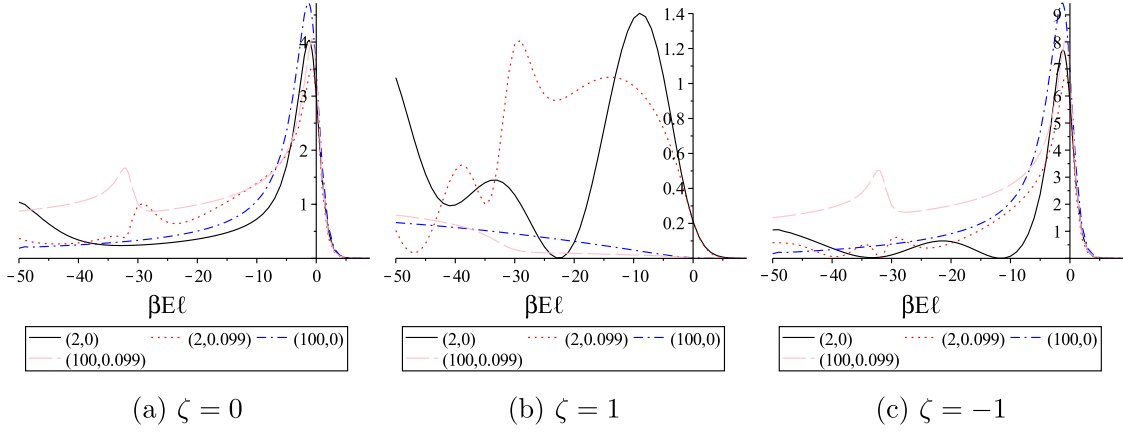


FIG. 5 (color online).  $\dot{\mathcal{F}}$  as a function of  $\beta E \ell$  for  $r_+/\ell = 0.1$ , with selected values of the pair  $(\alpha, r_-/\ell)$  as shown in the legend. Numerical evaluation from (5.6) with  $n \leq 35$ .

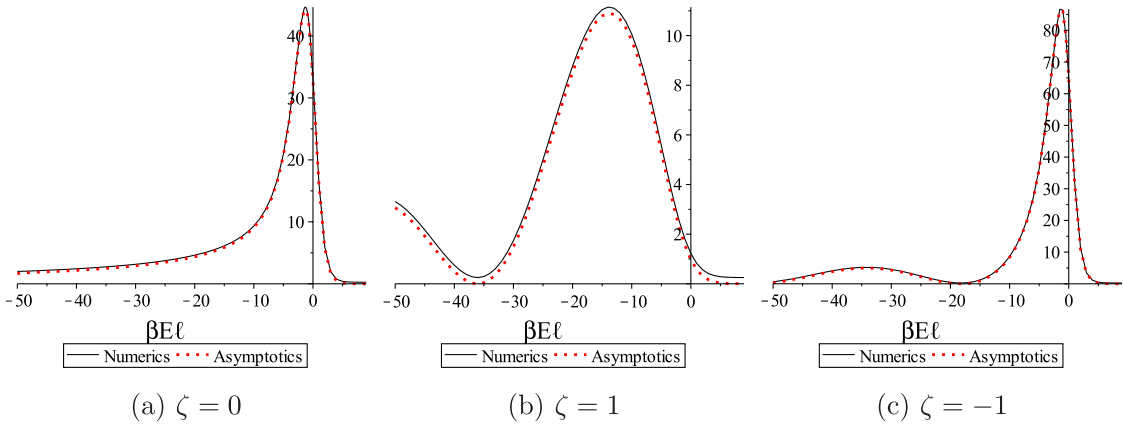


FIG. 6 (color online).  $\dot{\mathcal{F}}$  as a function of  $\beta E \ell$  for  $r_+/\ell = 0.01$  and  $r_- = 0$ , with  $\alpha = 4$ . Solid curve shows numerical evaluation from (5.6) with  $n \leq 300$ . Dotted curve shows the asymptotic small  $r_+/\ell$  approximation (5.10). Qualitatively similar graphs ensue for  $r_-/r_+ = 0.99$ .

## VI. RADIALLY IN-FALLING DETECTOR IN SPINLESS BTZ

In this section we consider a detector on a radially in-falling geodesic in a spinless BTZ spacetime.

### A. Transition rate

Recall from Sec. IV that for a spinless hole  $r_- = 0$  and  $r_+ = M\ell > 0$ , and the horizon is at  $r = r_+$ . To begin with, we assume that at least part of the trajectory is in the exterior region,  $r > r_+$ . Working in the exterior BTZ coordinates (4.3), the radial timelike geodesics take the form

$$r = \ell\sqrt{M}q\cos\tilde{\tau}, \quad t = (\ell/\sqrt{M})\operatorname{arctanh}\left(\frac{\tan\tilde{\tau}}{\sqrt{q^2-1}}\right),$$

$$\phi = \phi_0, \quad (6.1)$$

where  $q > 1$ ,  $\phi_0$  denotes the constant value of  $\phi$ , and  $\tilde{\tau}$  is an affine parameter such that the proper time equals  $\tilde{\tau}\ell$ . The additive constants in  $\tilde{\tau}$  and  $t$  have been chosen so that  $r$  reaches its maximum value  $\ell\sqrt{M}q$  at  $\tilde{\tau} = 0$  with  $t = 0$ .

Substituting (6.1) in (4.11) and (4.12), we find that the transition rate is given by

$$\dot{\mathcal{F}}_\tau(E) = 1/4 + \frac{1}{2\pi\sqrt{2}} \sum_{n=-\infty}^{\infty} \int_0^{\Delta\tilde{\tau}} d\tilde{s} \operatorname{Re} \left[ \frac{e^{-i\tilde{E}\tilde{s}}}{\sqrt{-1 + K_n \cos\tilde{\tau} \cos(\tilde{\tau} - \tilde{s}) + \sin\tilde{\tau} \sin(\tilde{\tau} - \tilde{s})}} \right. \\ \left. - \zeta \frac{e^{-i\tilde{E}\tilde{s}}}{\sqrt{1 + K_n \cos\tilde{\tau} \cos(\tilde{\tau} - \tilde{s}) + \sin\tilde{\tau} \sin(\tilde{\tau} - \tilde{s})}} \right], \quad (6.2)$$

where

$$K_n := 1 + 2q^2 \sinh^2(n\pi\sqrt{M}). \quad (6.3)$$

The detector is switched off at proper time  $\tau$  and switched on at proper time  $\tau_0 = \tau - \Delta\tau$ , and we have written  $\tilde{\tau} := \tau/\ell$ ,  $\Delta\tilde{\tau} := \Delta\tau/\ell$  and  $\tilde{E} := E\ell$ . The square roots in (6.2) are positive when the arguments are positive, and they are analytically continued to negative values of the arguments by giving  $\tilde{s}$  a small negative imaginary part.

Although the above derivation of (6.2) proceeded using the exterior BTZ coordinates, the result (6.2) holds by analytic continuation even if the geodesic enters the black or white hole regions. The ranges of the parameters are  $-\pi/2 < \tilde{\tau} - \Delta\tilde{\tau} < \tilde{\tau} < \pi/2$ , so that the detector is switched on after emerging from the white hole singularity and switched off before hitting the black hole singularity.

### B. The $n = 0$ term and KMS

We write (6.2) as

$$\dot{\mathcal{F}}_\tau = \dot{\mathcal{F}}_\tau^{n=0} + \dot{\mathcal{F}}_\tau^{n \neq 0}, \quad (6.4)$$

where  $\dot{\mathcal{F}}_\tau^{n=0}$  consists of the  $n = 0$  term and  $\dot{\mathcal{F}}_\tau^{n \neq 0}$  consists of the sum  $\sum_{n \neq 0}$ . We consider first  $\dot{\mathcal{F}}_\tau^{n=0}$ .

$\dot{\mathcal{F}}_\tau^{n=0}$  gives the transition rate of a detector on a geodesic in pure AdS<sub>3</sub>.  $\dot{\mathcal{F}}_\tau^{n=0}$  does not depend on  $M$  or  $q$ , and it depends on the switch-on and switch-off moments only through  $\Delta\tilde{\tau}$ , that is, through the total detection time. Using (6.2) and (6.3), we find

$$\dot{\mathcal{F}}_\tau^{n=0}(E) = \frac{1}{4} - \frac{1}{4\pi} \int_0^{\Delta\tilde{\tau}} d\tilde{s} \left[ \frac{\sin(\tilde{E}\tilde{s})}{\sin(\tilde{s}/2)} + \zeta \frac{\cos(\tilde{E}\tilde{s})}{\cos(\tilde{s}/2)} \right], \quad (6.5)$$

where  $\tilde{E} := E\ell$ . As  $0 < \Delta\tilde{\tau} < \pi$ , (6.5) is well defined.

The numerical examination shows that  $\dot{\mathcal{F}}_\tau^{n=0}$  does not satisfy the KMS condition. This is compatible with the embedding space discussion of Refs. [33–36], according to which a stationary detector in AdS<sub>3</sub> should respond thermally only when its scalar proper acceleration exceeds  $1/\ell$ .

The asymptotic behavior of  $\dot{\mathcal{F}}_\tau^{n=0}$  at large positive and negative energies for fixed  $\Delta\tilde{\tau}$  can be found by the method of Appendix E. We find

$$\dot{\mathcal{F}}_\tau^{n=0}(E) = \frac{\Theta(-\tilde{E})}{2} + \frac{1}{4\pi\tilde{E}} \left( \frac{\cos(\tilde{E}\Delta\tilde{\tau})}{\sin(\Delta\tilde{\tau}/2)} - \zeta \frac{\sin(\tilde{E}\Delta\tilde{\tau})}{\cos(\Delta\tilde{\tau}/2)} \right) + O(1/\tilde{E}^2), \quad (6.6)$$

where  $\Theta$  is the Heaviside step function.

### C. The $n \neq 0$ terms and large $M$ asymptotics

We now turn to  $\dot{\mathcal{F}}_\tau^{n \neq 0}$ , which contains the dependence of  $\dot{\mathcal{F}}_\tau$  on  $M$  and  $q$ .

We consider  $\dot{\mathcal{F}}_\tau^{n \neq 0}$  in the limit of large  $M$ . We introduce a positive constant  $c \in (0, \pi/2)$ , and we assume that the switch-on and switch-off moments are separated from the

initial and final singularities at least by proper time  $c\ell$ . In terms of  $\tilde{\tau}$  and  $\Delta\tilde{\tau}$ , this means that we assume

$$\begin{aligned} -\pi/2 + c < \tilde{\tau} < \pi/2 - c, \\ 0 < \Delta\tilde{\tau} < \tilde{\tau} + \pi/2 - c. \end{aligned} \quad (6.7)$$

As  $K_n = K_{-n}$ , we can replace the sum  $\sum_{n \neq 0}$  in (6.2) by  $2 \sum_{n=1}^{\infty}$ . Given (6.7), the expression  $\cos\tilde{\tau} \cos(\tilde{\tau} - \tilde{s})$  is bounded below by a positive constant. Using (6.3), this implies that the quantities under the  $n \neq 0$  square roots in (6.2) are dominated at large  $M$  by the term that involves  $K_n$ , and we may write

$$\begin{aligned} \dot{\mathcal{F}}_\tau^{n \neq 0}(E) &= \frac{1}{\pi\sqrt{2}\cos\tilde{\tau}} \sum_{n=1}^{\infty} \frac{1}{\sqrt{K_n}} \int_0^{\Delta\tilde{\tau}} \frac{\cos(\tilde{E}\tilde{s})d\tilde{s}}{\sqrt{\cos(\tilde{\tau} - \tilde{s})}} \\ &\times \left( \frac{1}{\sqrt{1 + f_-/K_n}} - \frac{\zeta}{\sqrt{1 + f_+/K_n}} \right), \end{aligned} \quad (6.8)$$

where

$$f_{\pm} := \frac{\sin\tilde{\tau} \sin(\tilde{\tau} - \tilde{s}) \pm 1}{\cos\tilde{\tau} \cos(\tilde{\tau} - \tilde{s})}. \quad (6.9)$$

The large  $M$  expansion of  $\dot{\mathcal{F}}_\tau^{n \neq 0}$  is then obtained by a binomial expansion of the square roots in (6.8) at  $K_n \rightarrow \infty$  and using (6.3). The expansion is uniform in  $\tilde{\tau}$  and  $\Delta\tilde{\tau}$  within the range (6.7), and by (6.3) it is also uniform in  $q$ . The first few terms are

$$\begin{aligned} \dot{\mathcal{F}}_\tau^{n \neq 0}(E) &= \frac{1}{\pi\sqrt{2}\cos\tilde{\tau}} \int_0^{\Delta\tilde{\tau}} \frac{\cos(\tilde{E}\tilde{s})d\tilde{s}}{\sqrt{\cos(\tilde{\tau} - \tilde{s})}} \\ &\times \left[ (1 - \zeta) \left( \frac{1}{\sqrt{K_1}} + \frac{1}{\sqrt{K_2}} \right) + \frac{\zeta f_+ - f_-}{2K_1^{3/2}} \right] \\ &+ O(e^{-5\pi\sqrt{M}}). \end{aligned} \quad (6.10)$$

For  $\zeta \neq 1$ , the dominant contribution comes from the term proportional to  $(1 - \zeta)$  and is of order  $e^{-\pi\sqrt{M}}$ .

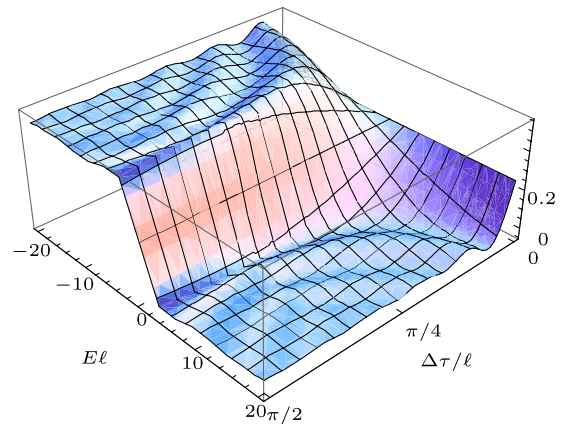


FIG. 7 (color online).  $\dot{\mathcal{F}}_\tau^{n=0}$  (6.5) as a function of  $E\ell$  and  $\Delta\tau/\ell$  for  $\zeta = 0$ .

### D. Numerical results

At large  $M$ , the dominant contribution to  $\dot{\mathcal{F}}_\tau$  comes from  $\dot{\mathcal{F}}_\tau^{n=0}$  (6.5), which depends only on  $E\ell$  and  $\Delta\tau/\ell$ . Plots are shown in Figs. 7 and 8. When  $|E\ell|$  is large, the oscillatory dependence on  $\Delta\tau/\ell$  shown in the plots is in agreement with the asymptotic formula (6.6).

When  $M$  decreases, the contribution to  $\dot{\mathcal{F}}_\tau$  from  $\dot{\mathcal{F}}_\tau^{n \neq 0}$  becomes significant. For  $M = 0.1$ , the terms shown in (6.10) are still a good fit to the numerics provided both the switch-on and the switch-off are in the exterior region. For smaller  $M$ , the number of terms that need to be included in  $\dot{\mathcal{F}}_\tau^{n \neq 0}$  increases rapidly. A set of plots is shown in Figs. 9 and 10 for  $M = 10^{-4}$  with  $q = 100$ , taking the detector to be switched on at the moment where  $r$  reaches its maximum and following the detector over a significant

fraction of its fall towards the horizon.  $\dot{\mathcal{F}}_\tau^{n \neq 0}$  turns out to be still insignificant at large negative  $E\ell$ , but it starts to become significant at  $E\ell \gtrsim -5$ , and its effect then depends strongly on the boundary condition parameter  $\zeta$ , being the smallest for  $\zeta = 1$ .

For fixed  $M$ , following the detector close to the future singularity numerically would pose two complications. First, an increasingly large number of terms would need to be included in  $\dot{\mathcal{F}}_\tau^{n \neq 0}$ . Second, the evaluation of the individual terms to sufficient accuracy would need to handle numerically integration over an integrable singularity in  $\tilde{s}$ . This singularity arises because the quantity under the first square root in (6.2) can change sign within the integration interval. We have not pursued this numerical problem.

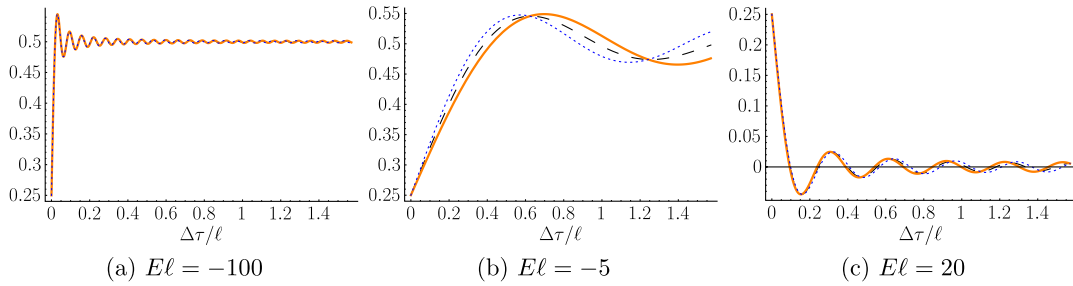


FIG. 8 (color online).  $\dot{\mathcal{F}}_\tau^{n=0}$  (6.5) as a function  $\Delta\tau/\ell$  for selected values of  $E\ell$ , with  $\zeta = 0$  (dashed line),  $\zeta = 1$  (thick line), and  $\zeta = -1$  (dotted line).

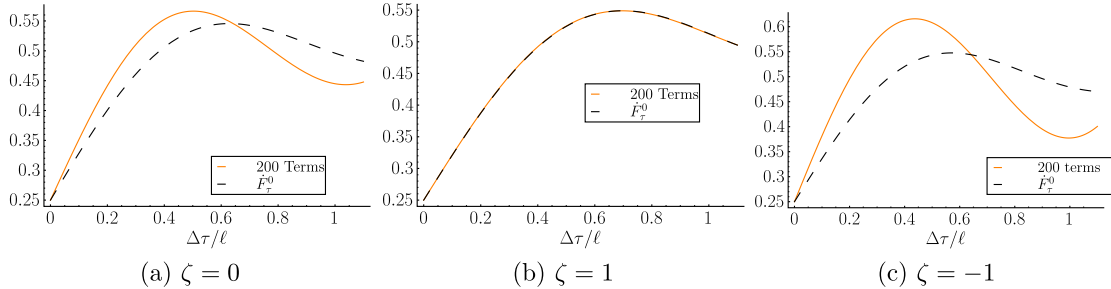


FIG. 9 (color online).  $\dot{\mathcal{F}}_\tau$  (6.2) with  $M = 10^{-4}$ ,  $q = 100$ ,  $\tau_0 = 0$ , and  $E\ell = -5$ . Solid line shows numerical evaluation from (6.2) with 200 terms and dashed line shows the individual  $n = 0$  term  $\dot{\mathcal{F}}_\tau^{n=0}$  (6.5). The horizon crossing occurs outside the plotted range, at  $\Delta\tau/\ell = \arccos(0.01) \approx 1.56$ .

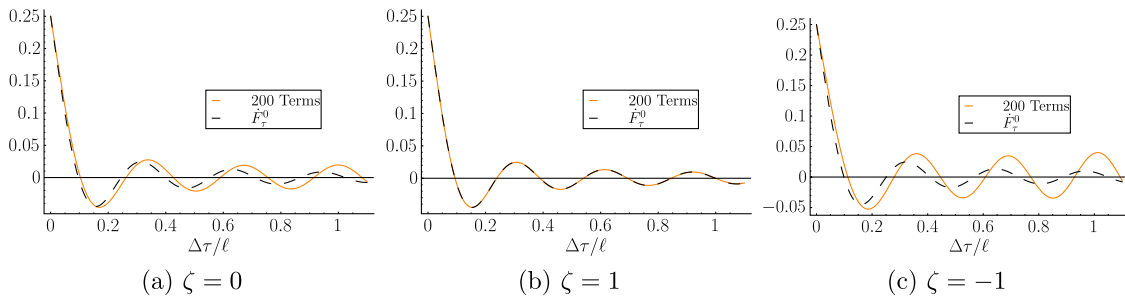


FIG. 10 (color online). As in Fig. 9 but with  $E\ell = 20$ .

## VII. CONCLUSIONS

In this paper we have investigated the response of an Unruh-DeWitt particle detector in three-dimensional curved spacetime. We first obtained a regulator-free expression for the transition probability of a detector coupled to a scalar field in an arbitrary Hadamard state, working within first-order perturbation theory and assuming that the detector is switched on and off smoothly, and we showed that both the total transition probability and the instantaneous transition rate remain well defined when the switching becomes sharp. In the special case of a detector in Minkowski space, coupled to the Minkowski vacuum of a massless scalar field, these results reduce to those found in Ref. [25]. The results confirm that the sharp switching limit is qualitatively different between three and four spacetime dimensions even when the spacetime is curved; in four dimensions, the sharp switching limit yields a well-defined transition rate but a divergent transition probability [17,24].

We then specialized to a detector in the BTZ black hole spacetime, coupled to a massless conformally coupled scalar field in a Hartle-Hawking vacuum state with transparent, Dirichlet or Neumann boundary conditions at the infinity. For a stationary detector that is outside the horizon and corotating with the hole, and switched on in the asymptotic past, we verified that the transition rate is thermal in the sense of the KMS property, in the local Hawking temperature that is determined by the mass and angular momentum of the hole and by the Tolman redshift factor at the detector's location. This is the temperature that was to be expected by general properties of the Hartle-Hawking state [6,7,28,32], and by GEMS considerations [33–36]. A static detector outside a nonrotating black hole was included as a special case. We obtained analytic results for the transition rate in a number of asymptotic regimes of the parameter space, including those of large and small black hole mass, and we provided numerical results in the interpolating regimes. We have not pursued in detail the case of a stationary detector whose angular velocity differs from that of the hole, but we shall show in Appendix F that the parameter space has at least some regimes in which the response of such a detector does not have the KMS property.

We also considered a detector that falls into a nonrotating BTZ hole along a radial geodesic. As the trajectory is not stationary, the transition rate is not constant along the trajectory, and, in particular, the switch-on cannot be pushed to the asymptotic past since the trajectory originates at the white hole singularity. We obtained analytic results for the transition rate when the black hole mass is large, and we evaluated the transition rate numerically for small values of the black hole mass provided the switch-on and switch-off take place in the exterior. We found no parameter ranges where the transition rate would be approximately thermal in the sense of the KMS property, not even near the moment of maximum radius on a trajectory, and we traced the reasons for this to the properties of  $\text{AdS}_3$  geodesics that have been

previously analyzed from GEMS considerations [33–36]. Our expression for the transition rate as a countable sum remains valid after the detector crosses the horizon, but the sum becomes then more difficult to estimate analytically and more labor intensive to evaluate numerically, and we have not pursued a detailed investigation of this regime.

It would be interesting to compare our BTZ transition rates to those of a detector on similar trajectories in four-dimensional Schwarzschild spacetime, where the Wightman function needs to be evaluated fully numerically. Some differences can be expected to arise from the different asymptotic infinities of BTZ and Schwarzschild: for example, an inertial detector in Schwarzschild should respond to the Hartle-Hawking vacuum approximately thermally in the asymptotically flat region. We leave this question as a subject for future work.

## ACKNOWLEDGMENTS

We thank Stephen Creagh for useful discussions on asymptotic techniques and Paul Townsend for bringing [36] to our attention. J.L. thanks the organizers of the “Bits, Branes, Black Holes” program for hospitality at the Kavli Institute for Theoretical Physics, University of California at Santa Barbara. This research was supported in part by the National Science Foundation under Grant No. NSF PHY11-25915. J.L. was supported in part by the Science and Technology Facilities Council.

## APPENDIX A: DERIVATION OF (5.5) AND (5.6)

In this appendix we verify the passage from (5.3) to (5.5) and (5.6).

### 1. $n = 0$ term

Let

$$I(a, P) := \text{Re} \int_0^\infty \frac{e^{-iax} dx}{\sqrt{P - \sinh^2 x}}, \quad (\text{A1})$$

where  $a \in \mathbb{R}$ ,  $P \geq 0$ , and the square root is positive for positive argument and positive imaginary for negative argument. We shall show that

$$I(a, 0) = -\frac{\pi \tanh(\pi a/2)}{2}, \quad (\text{A2a})$$

$$I(a, P) = e^{-\pi a/2} \int_0^\infty \frac{\cos(ay) dy}{\sqrt{P + \cosh^2 y}} \quad \text{for } P > 0. \quad (\text{A2b})$$

Applying (A2) and (A3) and to the  $n = 0$  term in (5.3) yields the corresponding terms in (5.5) and (5.6).

Suppose first  $P = 0$ . For  $P = 0$ , (A1) reduces to  $I(a, 0) = -\int_0^\infty \frac{\sin(ax)}{\sinh x} dx$ , which evaluates to (A2a) [39].

We note in passing the relation

$$I(a, 0) = -\frac{\pi}{2} + e^{-\pi a/2} \int_0^\infty \frac{\cos(ay) dy}{\cosh y}, \quad (\text{A3})$$

which follows by evaluating the integral in (A3) [39] and using (A2a). Comparison of (A2b) and (A3) shows that  $I(a, P)$  is not continuous at  $P = 0$ .

Suppose then  $P > 0$ . We rewrite (A1) as the contour integral

$$I(a, P) := \text{Re} \int_{C_1} \frac{e^{-iaz} dz}{\sqrt{P - \sinh^2 z}}, \quad (\text{A4})$$

where the contour  $C_1$  goes from  $z = 0$  to  $z = \infty$  along the positive real axis, with a dip in the lower half plane near the branch point  $z = \text{arcsinh} \sqrt{P}$ . The square root denotes the branch that is positive for small positive  $z$ .

We deform  $C_1$  into the union of  $C_2$  and  $C_3$ , where  $C_2$  goes from  $z = 0$  to  $z = -i\pi/2$  along the negative imaginary axis and  $C_3$  consists of the half line  $z = y - i\pi/2$  with  $0 \leq y < \infty$ . As the integrand has no singularities within the strip  $-\pi/2 \leq \text{Im } z < 0$  and falls off exponentially within this strip as  $\text{Re } z \rightarrow +\infty$ , the deformation does not change the value of the integral. The contribution from  $C_2$  is purely imaginary and vanishes on taking the real part. The contribution from  $C_3$  yields (A2b).

## 2. $n \neq 0$ terms

Let

$$I_b(a, P) := \text{Re} \int_0^\infty \frac{e^{-iax} dx}{\sqrt{P - \sinh^2(x+b)}}, \quad (\text{A5})$$

where  $a \in \mathbb{R}$ ,  $P > 0$ ,  $b \in \mathbb{R}$  and the square root is positive for positive argument and analytically continued to negative values of the argument by giving  $x$  a small negative imaginary part.

We shall show that

$$I_b(a, P) + I_{-b}(a, P) = 2 \cos(ab) I(a, P), \quad (\text{A6})$$

where  $I(a, P)$  is given in (A2b). Applying (A6) with (A2b) to the  $n \neq 0$  terms in (5.3) yields the corresponding terms in (5.5) and (5.6).

For  $b = 0$ , (A6) follows from (A2b). As both sides of (A6) are even in  $b$ , it hence suffices to consider (A6) for  $b > 0$ .

Let  $b > 0$ . Changing the integration variable in (A5) to  $y = x + b$  yields

$$\begin{aligned} I_b(a, P) + I_{-b}(a, P) &= 2 \cos(ab) \text{Re} \int_0^\infty \frac{e^{-ia y} dy}{\sqrt{P - \sinh^2 y}} \\ &\quad - \text{Re} \left( e^{iab} \int_0^b \frac{e^{-ia y} dy}{\sqrt{P - \sinh^2 y}} \right. \\ &\quad \left. + e^{-iab} \int_0^{-b} \frac{e^{-ia y} dy}{\sqrt{P - \sinh^2 y}} \right), \end{aligned} \quad (\text{A7})$$

where the branches of the square roots are as inherited from (A5): positive when the argument is positive and continued to negative argument by giving  $y$  a small negative imaginary part. Examination of the branches shows that the last two terms in (A7) cancel on taking the real part, and using (A1) in the first term leads to (A6).

## APPENDIX B: DERIVATION OF (5.9)

In this appendix we verify the asymptotic formula (5.9). Let

$$J(a, P) := \int_0^\infty \frac{\cos(ay) dy}{\sqrt{P + \cosh^2 y}}, \quad (\text{B1})$$

where  $P > 0$  and  $a \in \mathbb{R}$ . Note from (A2b) that  $I(a, P) = e^{-\pi a/2} J(a, P)$  for  $P > 0$ . We shall show that as  $P \rightarrow \infty$  with fixed  $a$ ,  $J(a, P)$  has the asymptotic form

$$\begin{aligned} J(a, P) &= \frac{1}{a\sqrt{\pi P}} \text{Im} \left[ (4P)^{ia/2} \Gamma(1 + ia/2) \Gamma\left(\frac{1}{2} - ia/2\right) \right] \\ &\quad + O(P^{-3/2}) \quad \text{for } a \neq 0, \end{aligned} \quad (\text{B2a})$$

$$\begin{aligned} J(0, P) &= \frac{1}{2\sqrt{P}} \left[ \ln(4P) + \psi(1) - \psi\left(\frac{1}{2}\right) \right] \\ &\quad + O(P^{-3/2} \ln P), \end{aligned} \quad (\text{B2b})$$

where  $\psi$  is the digamma function [40].

Starting from (B1), writing  $\cos(ay) = \text{Re}(e^{ia y})$  and making the substitution  $y = \ln t$ , we find

$$\begin{aligned} J(a, P) &= 2 \text{Re} \int_1^\infty \frac{t^{ia} dt}{\sqrt{t^4 + B^2 t^2} \sqrt{1 + \frac{1}{t^4 + B^2 t^2}}} \\ &= 2 \sum_{p=0}^\infty b_p \text{Re} \int_1^\infty \frac{t^{ia} dt}{t^{2p+1} (t^2 + B^2)^{p+(1/2)}}, \end{aligned} \quad (\text{B3})$$

where  $B = \sqrt{4P+2}$  and  $b_p$  are the coefficients in the binomial expansion  $(1+x)^{-1/2} = \sum_{p=0}^\infty b_p x^p$ . As the  $p > 0$  terms in (B3) are  $O(B^{-2p-1}) = O(P^{-p-(1/2)})$  by dominated convergence, we have  $J(a, P) = J_0(a, P) + O(P^{-3/2})$ , where the substitution  $t = Bv$  in the  $p = 0$  terms gives

$$J_0(a) = \frac{2}{B} \text{Re} \left( B^{ia} \int_{1/B}^\infty \frac{v^{ia-1} dv}{\sqrt{1+v^2}} \right). \quad (\text{B4})$$

When  $a \neq 0$ , integrating (B4) by parts and extending the lower limit of the integral to zero gives

$$J_0(a, P) = \frac{2}{Ba} \text{Im} \left[ B^{ia} \int_0^\infty \frac{v^{1+ia} dv}{(1+v^2)^{3/2}} + O(B^{-2}) \right]. \quad (\text{B5})$$

The integral in (B5) may be evaluated by writing  $(1+v^2)^{-3/2} = (\Gamma(3/2))^{-1} \int_0^\infty dx x^{1/2} e^{-(1+v^2)x}$  and interchanging the order of the integrals, with the result (B2a). When  $a = 0$ , similar manipulations lead to (B2b).

## APPENDIX C: DERIVATION OF (5.10)

Let  $p > 0$ ,  $q > 0$ ,  $a \in \mathbb{R}$ , and  $\gamma \in \mathbb{R}$ . For  $n \in \mathbb{Z}$ , let  $K_n := p^2 \sinh^2(nq)$ , and define

$$F_n := \int_0^\infty \frac{\cos(n\gamma q) \cos(ay) dy}{\sqrt{K_n + \cosh^2 y}}, \quad (\text{C1})$$



where we suppress the dependence of  $F_n$  on  $p, q, a$ , and  $\gamma$ . We shall show that the sum  $S := \sum_{n=-\infty}^{\infty} F_n$  has the asymptotic form

$$S = \frac{2}{q} \int_0^\infty dr \int_0^\infty \frac{\cos(r\gamma) \cos(ay) dy}{\sqrt{p^2 \sinh^2 r + \cosh^2 y}} + \frac{o(1)}{q}, \quad (\text{C2})$$

as  $q \rightarrow 0$  with the other parameters fixed. Note that the leading term in (C2) diverges as  $q \rightarrow 0$ .

Let

$$G(r) := \cos(\gamma r) \int_0^\infty \frac{\cos(ay) dy}{\sqrt{p^2 \sinh^2 r + \cosh^2 y}}, \quad (\text{C3})$$

where we suppress the dependence of  $G$  on  $a$  and  $\gamma$ .  $S$  then equals  $q^{-1}$  times the Riemann sum of  $G$  with the sampling points  $r = nq$ ,  $n \in \mathbb{Z}$ .  $G$  is continuous, and from Appendix B we see that  $|G(r)|$  is exponentially small as  $r \rightarrow \pm\infty$ . The Riemann sum of  $G$  therefore converges to the integral of  $G$  as  $q \rightarrow 0$ . Noting finally that  $G$  is even, we recover (C2).

#### APPENDIX D: COROTATING RESPONSE AT $E\ell \rightarrow \pm\infty$

In this appendix we analyze the individual terms in the corotating detector response (5.6) in the limit  $E\ell \rightarrow \pm\infty$ . These terms are of the form

$$\tilde{I}(\chi, a, P) := \cos(\chi a) e^{-\pi a/2} J(a, P), \quad (\text{D1})$$

where  $\chi \in \mathbb{R}$ ,  $a \in \mathbb{R}$ ,  $P > 0$  and  $J(a, P)$  is given by (B1). We shall show that when  $a \rightarrow \pm\infty$  with fixed  $\chi$  and  $P$ ,  $\tilde{I}(\chi, a, P)$  has the asymptotic expansion

$$\begin{aligned} \tilde{I}(\chi, a, P) &= \begin{cases} \frac{2\sqrt{\pi} e^{-\pi a} \cos(\chi a) \cos(\alpha a - \pi/4)}{\sqrt{a \sinh(2\alpha)}} + o(a^{-1/2} e^{-a\pi}) & a \rightarrow +\infty, \\ \frac{2\sqrt{\pi} \cos(\chi a) \cos(-\alpha a - \pi/4)}{\sqrt{-a \sinh(2\alpha)}} + o((-a)^{-1/2}) & a \rightarrow -\infty, \end{cases} \\ & \quad (\text{D2}) \end{aligned}$$

where  $\alpha = \text{arcsinh} \sqrt{P}$ .

Assuming  $a \neq 0$  and writing  $\cos(ay) = \text{Re}(e^{ialy})$ , we start by rewriting  $J(a, P)$  from (B1) as

$$J(a, P) = \text{Re} \int_{C_1} \frac{e^{ialy} dy}{\sqrt{P + \cosh^2 y}}, \quad (\text{D3})$$

where the contour  $C_1$  consists of the positive imaginary axis traveled downwards and the positive real axis traveled rightwards. The contribution from the imaginary axis vanishes on taking the real part.

Writing  $P = \sinh^2 \alpha$  where  $\alpha > 0$  and factorizing the quantity under the square root in (D3), we obtain

$$J(a, P) = \text{Re} \int_{C_1} \frac{e^{ialy} dy}{\sqrt{\sinh(\alpha + y - i\pi/2) \sinh(\alpha - y + i\pi/2)}}. \quad (\text{D4})$$

The branch points of the integrand in (D4) are at  $y = \pm\alpha + i\pi(n + \frac{1}{2})$ ,  $n \in \mathbb{Z}$ . We may deform  $C_1$  into the contour  $C_2$  that comes down from  $\alpha + i\infty$  at  $\text{Re } y = \alpha$ , passing the branch points from the left, encircles the branch point at  $y = \alpha + i\pi/2$  counterclockwise, and finally goes back up to  $\alpha + i\infty$  at  $\text{Re } y = \alpha$  but now passing the branch points from the right. Changing the integration variable by  $y = \alpha + i\pi/2 + iu$ , we then have

$$J(a, P) = e^{-|a|\pi/2} \text{Re} \left( i e^{ia|a|} \int_{C_3} \frac{e^{-|a|u} du}{\sqrt{-i \sin(u) \sinh(2\alpha + iu)}} \right), \quad (\text{D5})$$

where contour  $C_3$  comes from  $u = +\infty$  to  $u = 0$  on the upper lip of the positive  $u$  axis, encircles  $u = 0$  counterclockwise, and goes back to  $u = +\infty$  on the lower lip of the positive  $u$  axis. The square root is positive at  $u = \pi/2$  on the upper lip and it is analytically continued to the rest of  $C_3$ .

We now note that  $\sinh(2\alpha + iu) = \sinh(2\alpha) \cos(u) + i \cosh(2\alpha) \sin(u)$ , and that the modulus of this expression is bounded below by  $\sinh(2\alpha)$ . In (D5), the contribution from the two intervals in which  $\pi/2 \leq u \leq \pi$  is therefore bounded above by  $e^{-|a|\pi} / \sqrt{\sinh(2\alpha)}$  times a numerical constant, and the contribution from the two intervals in which  $n\pi \leq u \leq (n+1)\pi$ ,  $n = 1, 2, \dots$ , is bounded above by  $e^{-|a|\pi[n+(1/2)]} / \sqrt{\sinh(2\alpha)}$  times a numerical constant. The sum of all of these contributions is hence  $O(e^{-|a|\pi})$ . In the remaining contribution, coming from the two intervals in which  $0 \leq u \leq \pi/2$ , we combine the upper and lower lips and change the integration variable to  $w = |a|u$ . This gives

$$\begin{aligned} J(a, P) &= \frac{2e^{-|a|\pi/2}}{\sqrt{|a|}} \times \text{Re} \left( e^{i(\alpha|a| - \pi/4)} \int_0^{|a|\pi/2} \frac{e^{-w} dw}{\sqrt{|a| \sin(w/|a|) [\sinh(2\alpha) \cos(w/|a|) + i \cosh(2\alpha) \sin(w/|a|)]}} \right) \\ &\quad + O(e^{-|a|\pi}), \end{aligned} \quad (\text{D6})$$

where the square root denotes the branch that is positive in the limit  $w \rightarrow 0_+$ .

By Jordan's lemma, the modulus of the integrand in (D6) is bounded from above in the range of integration by the function  $g(w) := \sqrt{\frac{\pi}{2 \sinh(2\alpha)}} w^{-1/2} e^{-w}$ . As  $g(w)$  is integrable over  $0 < w < \infty$  and independent of  $a$ , dominated convergence guarantees that when  $|a| \rightarrow \infty$ , the limit in the integrand in (D6) can be taken under the integral. The integral that ensues in the limit is elementary, and we obtain

$$J(a, P) = \frac{2\sqrt{\pi} e^{-|a|\pi/2} \cos(\alpha|a| - \pi/4)}{\sqrt{|a| \sinh(2\alpha)}} + o(|a|^{-1/2} e^{-|a|\pi/2}). \quad (\text{D7})$$

(D2) then follows by substituting (D7) in (D1).

### APPENDIX E: DERIVATION OF (6.6)

In this appendix we verify the asymptotic expansions

$$\int_0^m dx \frac{\cos(\beta x)}{\cos x} = \frac{\sin(m\beta)}{\beta \cos m} + O(\beta^{-2}), \quad (\text{E1a})$$

$$\int_0^m dx \frac{\sin(\beta x)}{\sin x} = \frac{\pi \operatorname{sgn} \beta}{2} - \frac{\cos(m\beta)}{\beta \sin m} + O(\beta^{-2}), \quad (\text{E1b})$$

valid as  $\beta \rightarrow \pm\infty$  with fixed  $m \in (0, \pi)$ .

Equation (E1a) follows by repeated integrations by parts that bring down inverse powers of  $\beta$  [41].

In (E1b), we split the integral as

$$\begin{aligned} \int_0^m dx \left( \frac{1}{\sin x} - \frac{1}{x} \right) \sin(\beta x) - \int_m^\infty dx \frac{\sin(\beta x)}{x} \\ + \int_0^\infty dx \frac{\sin(\beta x)}{x}. \end{aligned} \quad (\text{E2})$$

Repeated integrations by parts now apply to the first two terms in (E2), and the third term equals  $\frac{\pi}{2} \operatorname{sgn} \beta$  [39]. Combining, we obtain (E1b).

### F. STATIONARY BUT NONCOROTATING DETECTOR

In this appendix we discuss briefly a detector that is stationary in the exterior region of the BTZ black hole but not corotating with the horizon. For the transparent boundary condition at the infinity, we show that the  $n=0$  term in the transition rate (4.11) breaks the KMS property already in second order in the difference between the horizon and detector angular velocities. As the  $n=0$  term is expected to give the dominant contribution when the black hole mass is large, we take

this as evidence that the transition rate does not satisfy the KMS property, in agreement with the GEMS prediction [33–36].

Consider a detector that is stationary in the exterior region of the BTZ spacetime at exterior BTZ coordinate  $r$ , but not necessarily corotating with the horizon. The tangent vector of the trajectory is a linear combination of  $\partial_t$  and  $\partial_\phi$ . By (4.3) and (4.4), the lift of the trajectory to  $\text{AdS}_3$  reads

$$\begin{aligned} X_1 &= \ell \cosh \chi \sinh(2ky), & T_1 &= \ell \cosh \chi \cosh(2ky), \\ X_2 &= \ell \sinh \chi \cosh(2y), & T_2 &= \ell \sinh \chi \sinh(2y), \end{aligned} \quad (\text{F1})$$

where we have written  $\sqrt{a} = \cosh \chi$  with  $\chi > 0$ , the constant  $k$  is proportional to the difference of the detector and horizon angular velocities, and  $y$  is a parameter along the trajectory. We assume  $|k| < \tanh \chi$ , which is the condition for the trajectory to be timelike. The proper time  $\tau$  is related by  $y$  by  $\tau = 2\ell \sinh \chi \sqrt{1 - k^2 \coth^2 \chi} y$ .

Let  $\hat{\mathcal{F}}^{n=0}$  denote the  $n=0$  term in the transition rate (4.11). Substituting (F1) in (4.12), and specializing to the transparent boundary condition,  $\zeta = 0$ , we find

$$\begin{aligned} \hat{\mathcal{F}}^{n=0}(E) &= \frac{1}{4} - \frac{1}{2\pi} \sqrt{1 - k^2 \coth^2 \chi} \\ &\times \int_0^\infty dy \frac{\sin(2E\ell \sinh \chi \sqrt{1 - k^2 \coth^2 \chi} y)}{\sqrt{\sinh^2 y - \coth^2 \chi \sinh^2(ky)}}. \end{aligned} \quad (\text{F2})$$

It can be verified that the quantity under the square root in the denominator is positive for  $0 < y < \infty$ .

Expanding (F2) as a power series in  $E$  and then expanding the coefficients as power series in  $k$ , we find

$$\begin{aligned} \hat{\mathcal{F}}^{n=0}(E) &= \frac{1}{4} + \left[ -\frac{\pi}{4} \sinh \chi + \frac{\pi}{8} \left( \frac{\pi^2}{4} - 1 \right) \right. \\ &\times \frac{\cosh^2 \chi}{\sinh \chi} k^2 + O(k^4) \left. \right] E\ell \\ &+ \left[ \frac{\pi^3}{12} \sinh^3 \chi + \frac{\pi^3}{4} \left( 1 - \frac{\pi^2}{6} \right) \right. \\ &\times \sinh \chi \cosh^2 \chi k^2 + O(k^4) \left. \right] (E\ell)^3 + O((E\ell)^5). \end{aligned} \quad (\text{F3})$$

From (F3) it is seen that the power series expansion of  $\hat{\mathcal{F}}^{n=0}(-E)/\hat{\mathcal{F}}^{n=0}(E)$  in  $E$  is incompatible with a pure exponential in  $E$ , and the discrepancy arises in the coefficient of the  $(E\ell)^3$  term in order  $k^2$ .  $\hat{\mathcal{F}}^{n=0}$  (F2) hence does not satisfy the KMS property at small but nonzero  $k$ .

- [1] W. G. Unruh, *Phys. Rev. D* **14**, 870 (1976).
- [2] B. S. DeWitt, in *General Relativity; An Einstein Centenary Survey*, edited by S. W. Hawking and W. Israel (Cambridge University Press, Cambridge, England, 1979) p. 680.
- [3] S. Takagi, *Prog. Theor. Phys. Suppl.* **88**, 1 (1986).
- [4] L. C. B. Crispino, A. Higuchi, and G. E. A. Matsas, *Rev. Mod. Phys.* **80**, 787 (2008).
- [5] S. W. Hawking, *Commun. Math. Phys.* **43**, 199 (1975); **46**, 206(E) (1976).
- [6] J. B. Hartle and S. W. Hawking, *Phys. Rev. D* **13**, 2188 (1976).
- [7] W. Israel, *Phys. Lett.* **57A**, 107 (1976).
- [8] G. W. Gibbons and S. W. Hawking, *Phys. Rev. D* **15**, 2738 (1977).
- [9] N. D. Birrell and P. C. W. Davies, *Quantum Fields in Curved Space* (Cambridge University Press, Cambridge, England, 1982).
- [10] R. M. Wald, *Quantum Field Theory in Curved Spacetime and Black Hole Thermodynamics* (University of Chicago Press, Chicago, 1994).
- [11] B. S. Kay and R. M. Wald, *Phys. Rep.* **207**, 49 (1991).
- [12] Y. Decanini and A. Folacci, *Phys. Rev. D* **73**, 044027 (2006).
- [13] C. J. Fewster, *Classical Quantum Gravity* **17**, 1897 (2000).
- [14] W. Junker and E. Schrohe, *Ann. Henri Poincaré* **3**, 1113 (2002).
- [15] L. Hörmander, *The Analysis of Linear Partial Differential Operators I (Distribution Theory and Fourier Analysis)* (Springer, Berlin, 1990), 2nd ed., Theorem 8.2.4.
- [16] L. Hörmander, *Acta Math.* **127**, 79 (1971), Theorem 2.5.11'; Reprinted in: J. Brüning and V. W. Guillemin, *Fourier Integral Operators* (Springer, Berlin, 1994).
- [17] J. Louko and A. Satz, *Classical Quantum Gravity* **25**, 055012 (2008).
- [18] L. Sriramkumar and T. Padmanabhan, *Classical Quantum Gravity* **13**, 2061 (1996).
- [19] S. Schlicht, *Classical Quantum Gravity* **21**, 4647 (2004).
- [20] S. Schlicht, Ph.D. thesis, University of Freiburg, 2002.
- [21] P. Langlois, *Ann. Phys. (N.Y.)* **321**, 2027 (2006).
- [22] P. Langlois, [arXiv:gr-qc/0510127](https://arxiv.org/abs/gr-qc/0510127).
- [23] J. Louko and A. Satz, *Classical Quantum Gravity* **23**, 6321 (2006).
- [24] A. Satz, *Classical Quantum Gravity* **24**, 1719 (2007).
- [25] L. Hodgkinson and J. Louko, *J. Math. Phys. (N.Y.)* **53**, 082301 (2012).
- [26] M. Bañados, C. Teitelboim, and J. Zanelli, *Phys. Rev. Lett.* **69**, 1849 (1992).
- [27] M. Bañados, M. Henneaux, C. Teitelboim, and J. Zanelli, *Phys. Rev. D* **48**, 1506 (1993).
- [28] G. Lifschytz and M. Ortiz, *Phys. Rev. D* **49**, 1929 (1994).
- [29] S. Carlip, *Classical Quantum Gravity* **12**, 2853 (1995).
- [30] R. Kubo, *J. Phys. Soc. Jpn.* **12**, 570 (1957).
- [31] P. C. Martin and J. S. Schwinger, *Phys. Rev.* **115**, 1342 (1959).
- [32] G. W. Gibbons and S. W. Hawking, *Phys. Rev. D* **15**, 2752 (1977).
- [33] S. Deser and O. Levin, *Classical Quantum Gravity* **14**, L163 (1997).
- [34] S. Deser and O. Levin, *Classical Quantum Gravity* **15**, L85 (1998).
- [35] S. Deser and O. Levin, *Phys. Rev. D* **59**, 064004 (1999).
- [36] J. G. Russo and P. K. Townsend, *Classical Quantum Gravity* **25**, 175017 (2008).
- [37] H. Ooguri, *Phys. Rev. D* **33**, 3573 (1986).
- [38] L. Sriramkumar, *Mod. Phys. Lett. A* **17**, 1059 (2002).
- [39] I. S. Gradshteyn and I. M. Ryzhik, *Tables of Integrals, Series and Products* (Academic Press, London, 2000), 6th ed.
- [40] Digital Library of Mathematical Functions (2012). National Institute of Standards and Technology, <http://dlmf.nist.gov/>.
- [41] R. Wong, *Asymptotic Approximations of Integrals* (Society for Industrial and Applied Mathematics, Philadelphia, 2001).